# Multiband Spectral Analysis and Faraday Synthesis of Abell 3395

W. D. Cotton (NRAO), I. Sihlangu (NRAO,SARAO) August 28, 2024

***Abstract*—This memo describes followup observations and analysis of a radio source in Abell cluster 3395 that showed complex Faraday spectra. This source is superposed on an X-ray emitting region and is suspected of interacting with it. The wavelength coverage of the original MeerKAT L band observations was insufficient to detect the really extended Faraday structures expected from a Jet-ICM interaction so additional MeerKAT observations were obtained at UHF and S Band. The expanded wavelength range of the combined data show the expected features extended in Faraday depth although still limited by the range of wavelength covered. The features being examined show strong depolarization towards the bottom of the observed range.**

***Index Terms*—Faraday Synthesis, Spectral Analysis**

## I. Introduction

LINEAR polarization observations over a range of wavelength of intrinsically polarized sources can reveal the Farday rotation in any intervening magnetized thermal plasma. A magnetized thermal plasma rotates the plane of a polarized signal passing through it by an amount, $\Delta\chi$ given by

$$\Delta\chi \;=\; \lambda^2\; 0.81 \int n_e B_{\parallel} dr, \qquad (1)$$

where $\lambda$ is the wavelength in m, $n_e$ is the electron density in $\mathrm{cm}^{-3}$, $B_{\parallel}$ is the strength of the component of the magnetic field along the line of sight in $\mu$Gauss and $r$ is distance in parsec.

If the source is entirely behind the rotating screen, the Faraday spectrum on a given sightline will show a single feature at a well defined “Rotation measure”. If the relativistic synchrotron emitting plasma is intermixed with the thermal, either macro- or micro-scopically, the Faraday spectrum may be more complex and show multiple and/or extended features.

The ability to recover extended features in the Faraday spectrum is limited by the wavelength coverage of the observations. As demonstrated in [1] and [2], a continious feature such as a top hat function which is sufficiently resolved in a given observation may be recovered as a pair of relatively narrow features at the ends of the extended feature. [1] and [2] featured observations of a source in galaxy cluster Abell 3395 which showed multiple feature in Faraday spectra made from MeerKAT L band observations. These works also demonstrate that with the available data, one cannot tell if there are multiple narrow features or multiple extended ones being resolved into multiple apparently narrow ones. Further MeerKAT observations in UHF band (600-1070 MHz) and S0 Band (1819-2600 MHz) were obtained to help understand this object better. This memo describes the analysis of this new data as well as the older L band data as analyzed in the Obit package [3][1] .

National Radio Astronomy Observatory, 520 Edgemont Rd., Charlottesville, VA, 22903 USA email: bcotton@nrao.edu

## II. Observations

### A. L Band (886-1680 MHz)

These observations, made as part of the survey of clusters of galaxies [4], used the center of the X ray emission (06 27 14.4 -54 28 12.) and were labeled J0627.2-5428. The observations were made on 2019–03–15 and 16 and were analysed as described in [4]. Calibration sources were J0408-6545, 1934-638 and J0538-4405. Stokes Q and U images were made in Obit task MFImage using a maximum fractional bandwidth (maxFBW) of 0.3% giving 223 channels across the bandpass. Many of these were totally blanked due to RFI removal.

### B. UHF (544-1088 MHz)

Abell 3395 was observed on 2023-10-26 with 7.6 hours on source and used J0408-6545, J0521+1638, J1331+3030 and J0538-4405 as calibrators. The pointing center used for UHF and S band was 06 26 49.4 -54 32 36. Sixty three of the sixty four antennas were used and all four correlations of the two orthogonal linear feeds were recorded. The bandpass was divided into 4096 channels with 8 second integrations. These observations used project code SCI-20230907-BC-01.

### C. S Band (1819-2600 MHz)

Abell 3395 was observed on 2023-11-03 with 7.5 hours on source and used J0408-6545, J0521+1638, J1331+3030 and J0538-4405 as calibrators. Fifty five of the 64 antennas were used and all four correlations of the two orthogonal linear feeds were recorded. The bandpass was divided into 4096 channels with 8 second integrations. These observations also used project code SCI-20230907-BC-01.

## III. Calibration

### A. L Band

The total intensity calibration is described in [4]. Since the observations did not contain a polarized calibrator, the polarization calibration depended on the noise diode calibration performed before the observations to correct the bulk of the X-Y phase offsets. J0538-4405 was used as the gain calibrator using a position of 05 38 50.184 -44 05 10.32. The residual X-Y phase offsets and the instrumental polarization terms were obtained from other, properly calibrated, datasets.

[1] http://www.cv.nrao.edu/∼bcotton/Obit.html

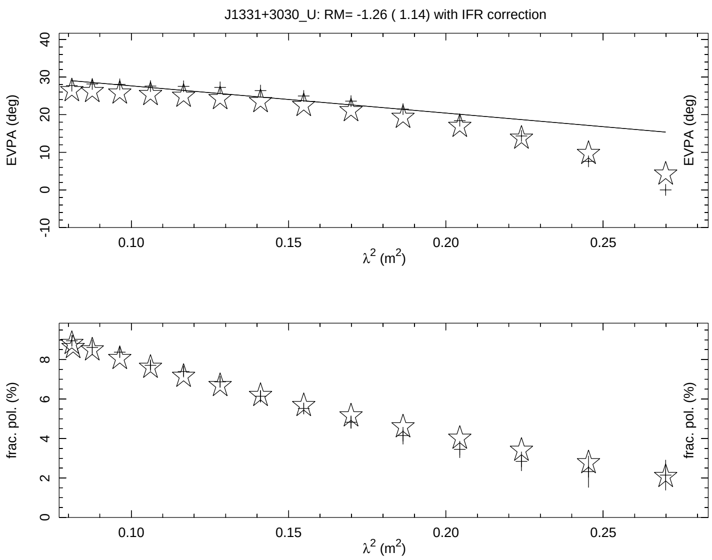


Fig. 1. Sub band EVPA and fractional polarization in UHF for J1331+3030 (3C286) after correction for ionospheric Faraday rotation.. Stars are the model values from [6]. The solid line is a rotation measure fit to the data.

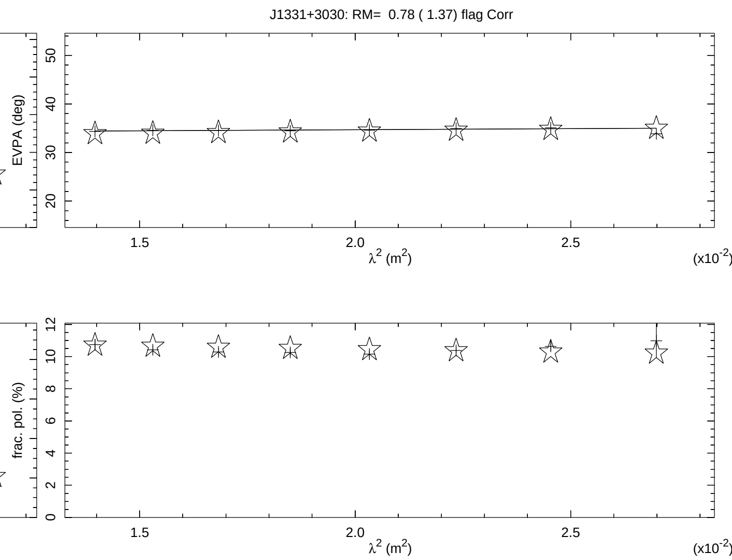


Fig. 2. Sub band EVPA and fractional polarization in S Band for J1331+3030 (3C286). Stars are the model values from [6].

### B. UHF

The total intensity calibration followed the general scheme of [4] using J0408-6545 as the flux density/delay/bandpass calibrator and J0538-4405 as the gain (astrometric) calibrator using a position of 05 38 50.36 -44 05 8.9.

At the time of the observations, the Sun was highly active leading to a disturbed ionosphere. This is especially bothersome at the low frequency of UHF band and the usual polarization calibration was inadequate and a modified procedure was used.

1) **X-Y phase and delay difference** The dataset contained two polarized calibrators J0521+1638 (3C138) and J1331+3030 (3C286), both of which are depolarizing at the bottom of UHF. Obit task RLDly was used to determine the X-Y phase and delay with calibrator J0521+1638.
2) **Instrumental Polarization** The instrumental polarization terms (ellipticity and orientation of the feeds) was then determined using Obit task PCal with 0408-6545 and J0538-4405 as unpolarized sources.
3) **Ionospheric Faraday Rotation** AIPS task TECOR was used to make corrections for the ionospheric Faraday rotation. This used the jplg (URL cddis.gsfc.nasa.gov) IONEX ionospheric model, TEC scale factor 0.85, an elevation scale of 0.978 and an elevation offset of 56.7 km. Details are described in [5].

The polarization calibration can be evaluated comparing the calibrated values for J1331+3030 with the model of [6] as shown in Figure 1. Since the single scan on J1331+3030 was at a low elevation and at a very different azimuth from Abell 3395, it may not be very representive for the data set as a whole.

### C. S Band

Total intensity calibration was as for UHF. For undetermined reasons, the polarization calibration scheme typically used for L band failed to give adequate calibration for the S band data and a modified procedure was used.

1) **Instrumental Polarization.** The instrumental polarization terms (ellipticity and orientation of the feeds) was determined using Obit task PCal with 0408-6545 and J0538-4405 as unpolarized sources.
2) **X-Y phase and delay difference.** The dataset contained two polarized calibrators J0521+1638 and J1331+3030. Since J1331+3030 has a good polarization model of the polarization [6]. it was used. A number of channels near the bottom of the band had discrepant cross hand values and were flagged. Then Obit task RLDly was used to determine the X-Y phase and delay using J1331+3030 per spectral window.
3) **Final calibration of X–Y phase using J1331+3030.** The above calibration resulted in significant errors (of order 30°) so a correction to the EVPA was determined from a comparison of a channel-by-channel average of all baselines and times for J1331+3030 with the model of [6]. This was done by applying the previous calibration to all J1331+3030 data and converting to a circular basis. Then Obit task AvgBL averaged all the data into a single spectrum. Script Abell3395_FixEVPA.py was used to create a BP table correcting the R–L phase; see Appendix. This BP table was applied to all data.

The polarization calibration can be evaluated comparing the calibrated values for J1331+3030 with the model of [6] as shown in Figure 2.

## IV. Imaging

Analysis used the L Band images from [4], [1] and [2]. L Band polarization imaging used maxFBW=0.003 giving 223 subband channels. All Imaging used Obit task MFImage [7].

### A. UHF

Imaging of the UHF data was done on workstation smeagle whose GPU was misbehaving and for more extended runs would crash the machine. Processing had to be sufficiently limited to avoid these crashes. (These should probably be redone. ) Imaging with doQU gives odd results for Stokes U; the Q and U Stokes parameters were imaged separately.

*1) Total Intensity:* The total intensity (Stokes I) imaging used the solutions from a phase only self calibration (A&P self cal went badly). Imaging used a field of view of radius 1.0° and a Robust factor of -2.5 to improve the resolution. The restoring beam was set to 9” $\times$ 9” although the fitted beam was slightly larger than 10”. The maxFBW of 0.05 gave 14 subband channels; the imaged field of view was 1°. CLEANing was to a depth of 100 $\mu$Jy/beam. Only phase self calibration was used; autoCen was not used.

*2) Linear Polarization:* In order to increase the range of Faraday depth accessable, the maxFBW was set to 0.3% which gave 222 subbands across the spectrum. Due to the GPU and doQU oddities for UPol, Q and U images were made in separate runs of MFImage. The spatial resolution and field of view imaged were the same as for total intensity. CLEANing proceeded to a depth of 50 $\mu$Jy/bm.

### B. S Band

Imaging at S band used a Robust factor of -0.5 to trade some resolution for sensitivity and get a resolution (5.8” $\times$ 5.1” @ -42.6°) closer to that of the lower frequencies.

*1) Total Intensity:* A field of view of radius 0.75° was imaged and CLEANed to a depth of 50 $\mu$Jy/bm. The maximum fractional bandwidth of 5% resulted in 8 subbands. Several cycles of phase only calibration was followed by an amplitude and phase self calibration. autoCen at 0.5 Jy was used to center a nearby, bright AGN in its own facet. Peeling was used to reduce the artifacts due to this nearby bright AGN.

*2) Linear Polarization:* A maximum fractional bandwidth (maxFBW) of 2% resulted in 20 subbands. A field of view of radius 0.5° was imaged and CLEANed to a depth of 50 $\mu$Jy/bm using joint Q & U deconvolution. A Robust factor of -1 resulted in a restoring beam of 4.5”.

## V. Astrometry

The various datasets were calibrated with the nearby gain calibrator, J0538-4405, but the position used was improved between the L band and UHF/S band observations; the older position being in error by several arcseconds. The L band image is thus not well aligned astrometrically with those of the other two bands. Fortunately, the field contains an ICRS source with a mas accuracy position and the source is strong and isolated in all the observed bands. This source is LCS J0625-5438 with RA (2000) 06 25 52.23060 and Dec (2000) -54 38 50.7049, and error 1.7 and 0.7 mas [8]. The L band image used a position about 2” from this while UHF and S band differed by only a couple hundred mas. The images were aligned using the following script fragments:

```
ras_L='06:25:52.08';decs_L='-54:38:52.4'# LBand
ras_S='06:25:52.22';decs_S='-54:38:50.6'# SBand
ras_U='06:25:52.25';decs_U='-54:38:50.4'# UHF
ras_icrs='06:25:52.23060';
decs_icrs='-54:38:50.7049' # ICRF position

# Per image
ra_obs=ras_L; dec_obs=decs_L  # LBand
ra_obs=ras_U; dec_obs=decs_U  # SBand
ra_obs=ras_S; dec_obs=decs_S  # UHF
cosdec=cos(radians(ImageDesc.PDMS2Dec(decs_icrs)))
ra_omi=(ImageDesc.PHMS2RA(ra_obs)- \
    ImageDesc.PHMS2RA(ras_icrs))*cosdec*3600
dec_omi=(ImageDesc.PDMS2Dec(dec_obs)- \
    ImageDesc.PDMS2Dec(decs_icrs))*3600
d=x.Desc.Dict  # Update descriptor ref. pixel
offx=(ra_omi/3600)/d['cdelt'][0];
offy=(dec_omi/3600)/d['cdelt'][1];
d['crpix'][0]+=offx; d['crpix'][1]+=offy
x.Desc.Dict=d
x.UpdateDesc(err)
```

TABLE I
Sources used for Flux Density Scaling

| Number | RA(2000) | Dec(2000) |
|---|---|---|
| 1 | 06 26 27.35 | -54 32 51.3 |
| 2 | 06 26 36.67 | -54 38 49.3 |
| 3 | 06 26 45.92 | -54 40 25.1 |
| 4 | 06 26 19.93 | -54 40 18.4 |
| 5 | 06 26 04.71 | -54 40 14.2 |
| 6 | 06 26 13.46 | -54 26 55.79 |
| 7 | 06 26 40.14 | -54 26 36.03 |
| 8 | 06 27 26.31 | -54 31 02.12 |
| 9 | 06 27 34.79 | -54 32 07.50 |
| 10 | 06 27 17.16 | -54 32 43.87 |
| 11 | 06 27 09.86 | -54 34 45.94 |
| 12 | 06 26 43.61 | -54 42 14.53 |

## VI. Photometry

The relative flux density scaling in the various bands was determined by fitting a spectrum to a selection of small, isolated, relatively strong sources and determining the average correction from the ratio of the subband flux densities at the position of the broadband peak to the value from the fitted spectrum. These sources are listed in Table I and the corrections derived and applied are given in Table II. The effect of the correction for one of the sources used is given in Figure 3.

## VII. Spectral Analysis

Section for Isaac.

## VIII. Faraday Synthesis

Faraday synthesis was performed using Obit task RMSyn which uses complex input files of the form produced by

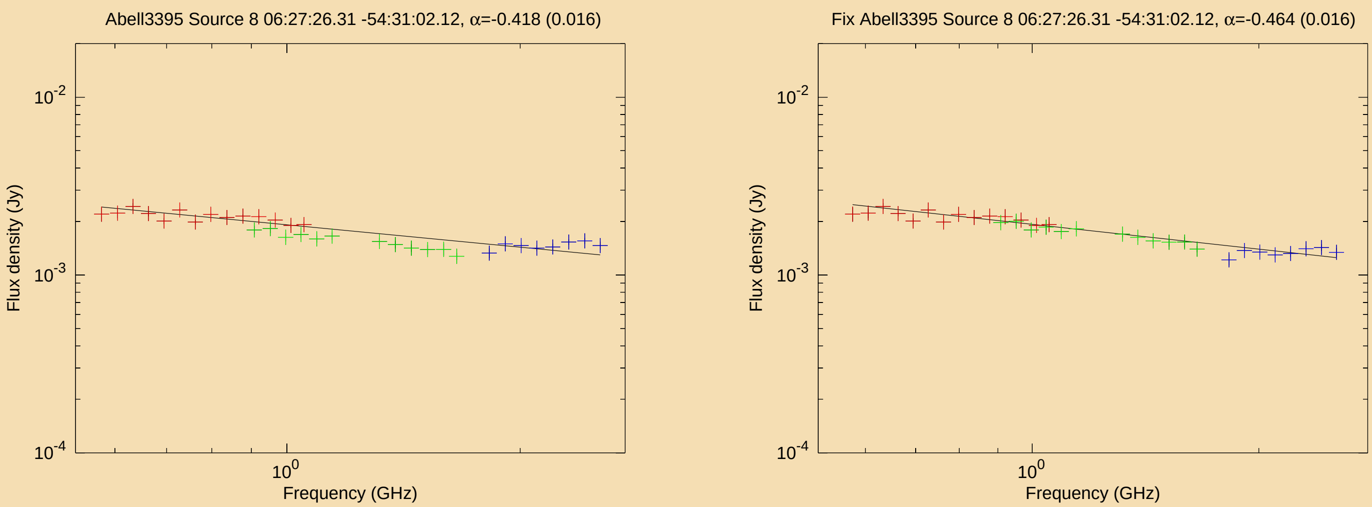


Fig. 3. Combined spectra of a bright source in the field, **Left:** As originally calibrated, **Right:** after rescaling Blue points are S Band, green are L band and red UHF. The solid line is a spectral fit with spectral index given in the title.

TABLE II
BAND FLUX DENSITY SCALING

| Band | Scaling Factor |
|---|---|
| UHF | 1.00 |
| L Band | 1.11 |
| S Band | 0.908 |

MFImage. The images in the different bands were also at different spatial resolutions and on different grids. The subbands with valid data were combined by the following procedure:

1) **Convolve to a common resolution.** The L and S band images have higher spatial resolution than UHF so the Q and U image cubes produced by MFImage were convolved to the same resolution (9" FWHM) as UHF using Obit task Convol.
2) **Regrid onto the same spatial grid.** Since the UHF and L band images were on a coarser grid than S Band, they were resampled using Obit task HGeom on the S band grid.
3) **Create combined MFImage–like images.** Existing Q and U MFImage type images are cloned into cubes with the desired number of subband planes for the combined data. This is done using share/scripts/scriptMakeMFCube.py.
4) **Populate combined Q and U cubes.** The valid subband planes and frequency information are copied from the various band MFImage Q and U images into the appropriate planes of the combined cubes. This uses share/scripts/CopyMFPlane.py.
5) **Faraday Synthesis.** Task RMSyn was run using the combined Q and U cubes to produce a Faraday spectra cube $\pm$1000 rad/m$^2$ in steps of 1 rad/m$^2$. Each spectrum was subjected to a complex CLEAN deconvolution and restored with a complex Gaussian whose amplitude had a $\sigma$=3.9 rad/m$^2$, the width fitted to the central lobe of the real part of the "dirty" psf. The "dirty" and restoring Faraday functions are shown in Figure 4.

Calibration is never perfect and at some level polarization images will be contaminated by artifacts from residual instrumental polarization. This will be especially important in cases like many of the sightlines discussed here for which the polarized emission is a small fraction of the total intensity. Fortunately, artifacts due to residual instrumental polarization behave very differently from Faraday rotation in wavelength squared and their effects tend to show up near 0 in Faraday spectra. Thus, Faraday synthesis can be one technique for reducing the effects of residual instrumental polarization when the Faraday depth varies from 0.

## IX. TESTS USING SIMULATED TOPHAT FARADAY DEPTH DISTRIBUTIONS

The main objective of combining data from the several frequency bands was to improve the ability to recover extended features in Faraday depth. [1] and [2] demonstrated the MeerKAT L Band data alone has difficulty distinguishing extended features from multiple narrow ones. Once a feature is well resolved, the central portion is "resolved out" and what is left is a pair of apparently narrow features. This is illustrated using the L Band coverage used here in Figure 5. This figure shows the derived, deconvolved, spectra for a series of tophat shaped features of varying width. For widths larger than about 50 rad/m$^2$ only a pair of narrow features remain.

The same simulation was performed using the wavelength coverage of the combined data and is shown in Figure 6. This figure shows increasing loss of sensitivity to the middle portion of the feature with increasing feature width but much less so than with the more restricted L band only coverage. The resolution in Faraday depth is also higher due to the inclusion of the longer wavelength UHF data.

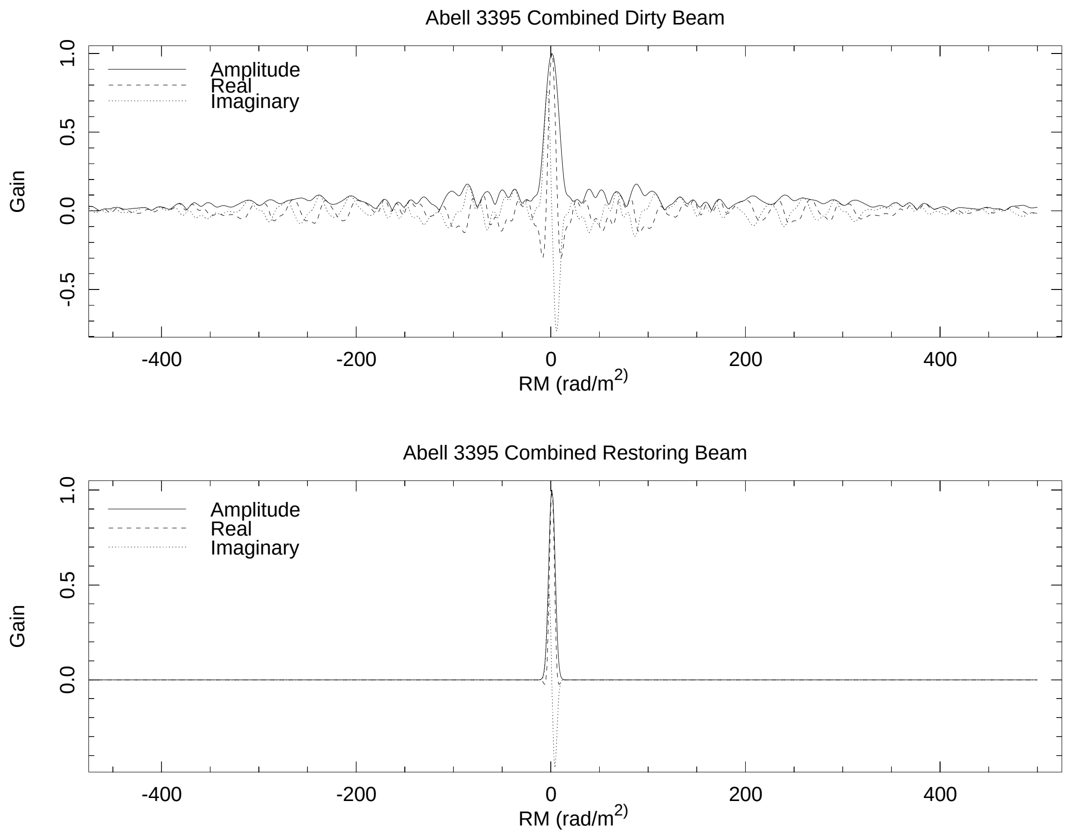


Fig. 4. The dirty and restoring resolution of Faraday synthesis of the combined UHF, L and S Band data. Upper plot is of the "dirty" psf and the lower gives the restoring function. Real, imaginary and amplitudes are shown as different line styles.

## X. Brightness and Spectral Index Distributions of Abell 3395

To be written by Isaac. see Figure 7.

## XI. Faraday Synthesis of Abell 3395

The combined Q and U image cubes were analyzed using task RMSyn and the deconvolved Faraday spectra investigated at a number of locations in the field of Abell cluster 3395. A contour map of the field in total intensity indicating the locations of Faraday spectra is displayed in Figure 8.

In order to evaluate the quality of the calibration of the data spectra of various AGNs and the cluster halo-like feature marked in Figure 8, Faraday spectra are given in Figure 9. This figure gives the combined spectrum as well as the spectra derived from each of the frequency band separately; there are four panels of four plots each. AGNs A and B are spatially unresolved while AGN C is well resolved. The Faraday spectrum of AGN A (upper right panel) has a single, narrow feature as expected. On the other hand, AGN B (upper right panel) which has a very inverted (i.e. optically thick) frequency spectrum appears strongly depolarized in the lower frequency bands. The strong, narrow feature near 0 rad/m$^2$ especially visible in the UHF spectrum is likely residual instrumental polarization. The spatially more complex AGN C shows multiple Faraday features. The sightline towards the halo-like feature is dominated by a single, narrow feature.

The extended FRII AGN jet on the left side of Figure 8 is mostly superposed on a region of X-ray emission (see Figure 11) except for the very southern end. Four locations in this source have Faraday spectra given in Figure 10. Except for the southernmost (jet feature D) the spectra show extended emission over several hundred rad/m$^2$. The combined spectra in features B and C are reminiscent of the resolved tophat features in Figure 6 with peaks at the ends of the extended feature and lower detected emission in the middle. Features A-C are also strongly depolarized with narrow lines near 0 rad/m$^2$ likely due to residual instrumental polarization. The Faraday features are not strongly depolarized at S band which caused the S band plots of Features A-C to go way off scale. The spectra of these parts of the jet are quite steep (see Figure 7).

### A. $\lambda^2$ and Faraday Space

Spectra in $\lambda^2$ and Faraday space are related by a Fourier transform and it can be instructive to examine several of these pairs of spectra. The simple case of AGN A is shown in Figure 12; it is a single, narrow peak in Faraday space and a linear ramp of EVPA in $\lambda^2$ space. More complex cases are shown in Figures 13 and 14 which are samples at two locations in the jet of the FRII AGN. In the right plot of these figures the solid line is the Faraday rotation fitted to only the SBand data. In Figure 12 **Right** the EVPA measurements (nearly) fall along the RM line whereas in the other two, the measurements

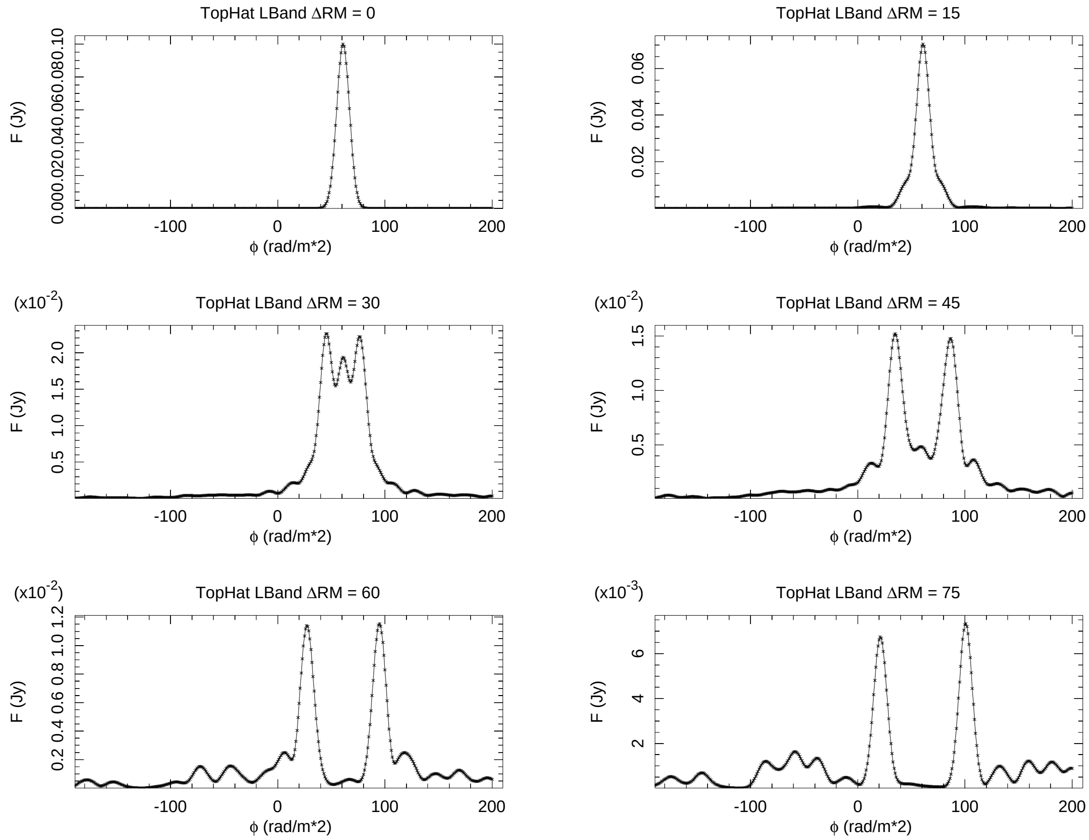


Fig. 5. The Faraday spectra of simulated MeerKAT observations at L band of a tophat function of various widths in Faraday depth. The feature is centered at 60 rad/m$^2$. The restoring Gaussian has a sigma of 6 rad/m$^2$.

at longer wavelengths show little correlation with the short wavelength RM fit. In the latter two Figures the increasing depolarization with increasing wavelength is very evident in the band plots on the left and the decreasing amplitude on the right. Figure 12 shows no evidence of depolarization but rather the steep spectrum of the source. The amplitude v. $\lambda^2$ function in Figures 13 and 14 **right** is similar to the sinc function that would be the result of a tophat in Faraday space.

## Appendix

The script used to determine EVLA corrections for S Band data (applied as R-L corrections) is given in Figure A.

## References

[1] W. D. Cotton and L. Rudnick, "Faraday Synthesis of Unequally Spaced Data and Complex Deconvolution," *Obit Development Memo Series*, vol. 76, pp. 1–18, 2022. [Online]. Available: https://www.cv.nrao.edu/∼bcotton/Obitdoc/RMSyn.pdf

[2] L. Rudnick and W. D. Cotton, "Correction to: Full resolution deconvolution of complex Faraday spectra," *MNRAS*, vol. 523, no. 1, pp. 774–774, Jul. 2023.

[3] W. D. Cotton, "Obit: A Development Environment for Astronomical Algorithms," *PASP*, vol. 120, pp. 439–448, 2008.

[4] K. Knowles, W. D. Cotton, L. Rudnick, F. Camilo, S. Goedhart, R. Deane, M. Ramatsoku, M. F. Bietenholz, M. Brüggen, C. Button, H. Chen, J. O. Chibueze, T. E. Clarke, F. de Gasperin, R. Ianjamasimanana, G. I. G. Józsa, M. Hilton, K. C. Kesebonye, K. Kolokythas, R. C. Kraan-Korteweg, G. Lawrie, M. Lochner, S. I. Loubser, P. Marchegiani, N. Mhlahlo, K. Moodley, E. Murphy, B. Namumba, N. Oozeer, V. Parekh, D. S. Pillay, S. S. Passmoor, A. J. T. Ramaila, S. Ranchod, E. Retana-Montenegro, L. Sebokolodi, S. P. Sikhosana, O. Smirnov, K. Thorat, T. Venturi, T. D. Abbott, R. M. Adam, G. Adams, M. A. Aldera, E. F. Bauermeister, T. G. H. Bennett, W. A. Bode, D. H. Botha, A. G. Botha, L. R. S. Brederode, S. Buchner, J. P. Burger, T. Cheetham, D. I. L. de Villiers, M. A. Dikgale-Mahlakoana, L. J. du Toit, S. W. P. Esterhuyse, G. Fadana, B. L. Fanaroff, S. Fataar, A. R. Foley, D. J. Fourie, B. S. Frank, R. R. G. Gamatham, T. G. Gatsi, M. Geyer, M. Gouws, S. C. Gumede, I. Heywood, M. J. Hlakola, A. Hokwana, S. W. Hoosen, D. M. Horn, J. M. G. Horrell, B. V. Hugo, A. R. Isaacson, J. L. Jonas, J. D. B. Jordaan, A. F. Joubert, R. P. M. Julie, F. B. Kapp, V. A. Kasper, J. S. Kenyon, P. P. A. Kotzé, A. G. Kotze, N. Kriek, H. Kriel, V. K. Krishnan, T. W. Kusel, L. S. Legodi, R. Lehmensiek, D. Liebenberg, R. T. Lord,

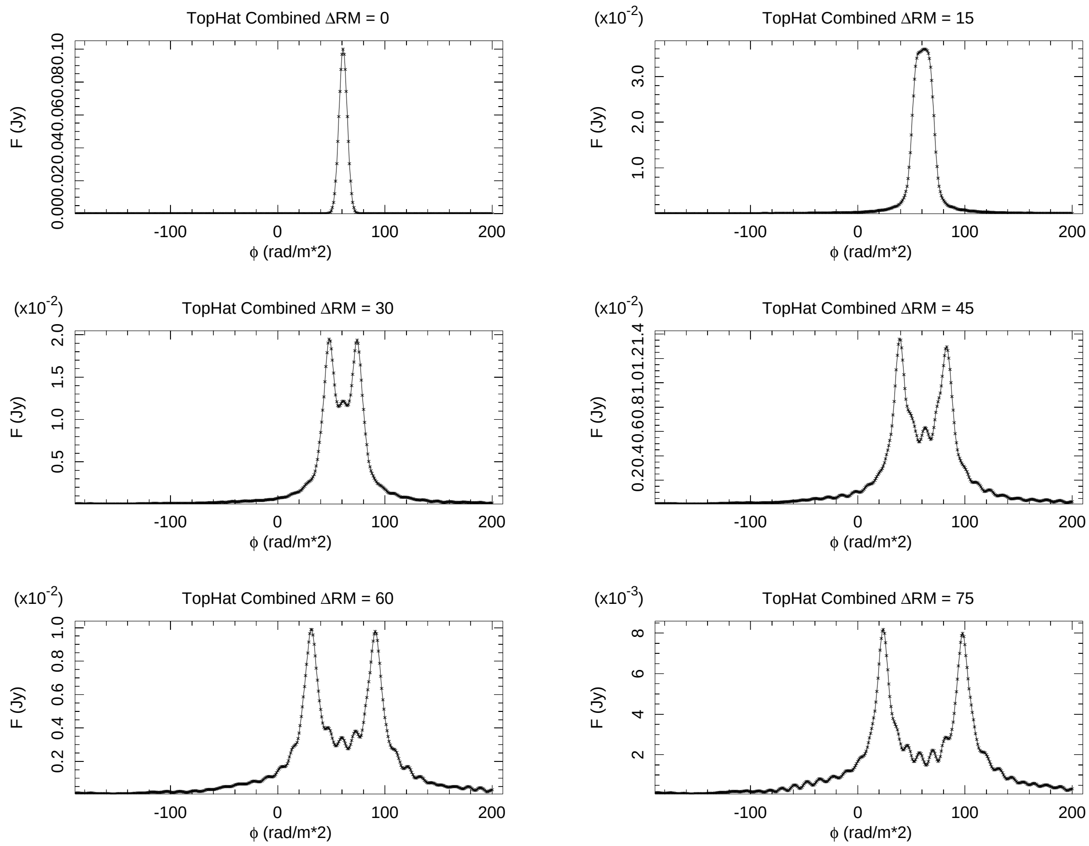


Fig. 6. The Faraday spectra of simulated MeerKAT observations combining UHF, L Band and S Band of a tophat function of various widths in Faraday depth. The feature is centered at 60 rad/m$^2$. The restoring Gaussian has a sigma of 3.9 rad/m$^2$.

B. M. Lunsky, K. Madisa, L. G. Magnus, J. P. L. Main, A. Makhaba, S. Makhathini, J. A. Malan, J. R. Manley, S. J. Marais, M. D. J. Maree, A. Martens, T. Mauch, K. McAlpine, B. C. Merry, R. P. Millenaar, O. J. Mokone, T. E. Monama, M. C. Mphego, W. S. New, B. Ngcebetsha, K. J. Ngoasheng, M. T. Ockards, A. J. Otto, A. A. Patel, A. Peens-Hough, S. J. Perkins, N. M. Ramanujam, Z. R. Ramudzuli, S. M. Ratcliffe, R. Renil, A. Robyntjies, A. N. Rust, S. Salie, N. Sambu, C. T. G. Schollar, L. C. Schwardt, R. L. Schwartz, M. Serylak, R. Siebrits, S. K. Sirothia, M. Slabber, L. Sofeya, B. Taljaard, C. Tasse, A. J. Tiplady, O. Toruvanda, S. N. Twum, T. J. van Balla, A. van der Byl, C. van der Merwe, C. L. van Dyk, V. Van Tonder, R. Van Wyk, A. J. Venter, M. Venter, M. G. Welz, L. P. Williams, and B. Xaia, "The MeerKAT Galaxy Cluster Legacy Survey. I. Survey Overview and Highlights," *A&A*, vol. 657, p. A56, Jan. 2022.

[5] W. D. Cotton, "Ionospheric Faraday Rotation Correction," *Obit Development Memo Series*, vol. 83, p. 1, 2024. [Online]. Available: https://www.cv.nrao.edu/∼bcotton/ObitDoc/IonTECor.pdf

[6] B. Hugo and R. Perley, "Absolute linear polarization angle calibration using planetary bodies for MeerKAT and JVLA at cm wavelengths," *SARAO documents*, vol. SSA-0004E-001, pp. 1–70, 2024.

[7] W. D. Cotton, J. J. Condon, K. I. Kellermann, M. Lacy, R. A. Perley, A. M. Matthews, T. Vernstrom, D. Scott, and J. V. Wall, ""The Angular Size Distribution of $\mu$jy Radio S"ources"," *ApJ*, vol. 856, p. 67, 2018.

[8] L. Petrov, A. de Witt, E. M. Sadler, C. Phillips, and S. Horiuchi, "The Second LBA Calibrator Survey of southern compact extragalactic radio sources - LCS2," *MNRAS*, vol. 485, no. 1, pp. 88–101, May 2019.

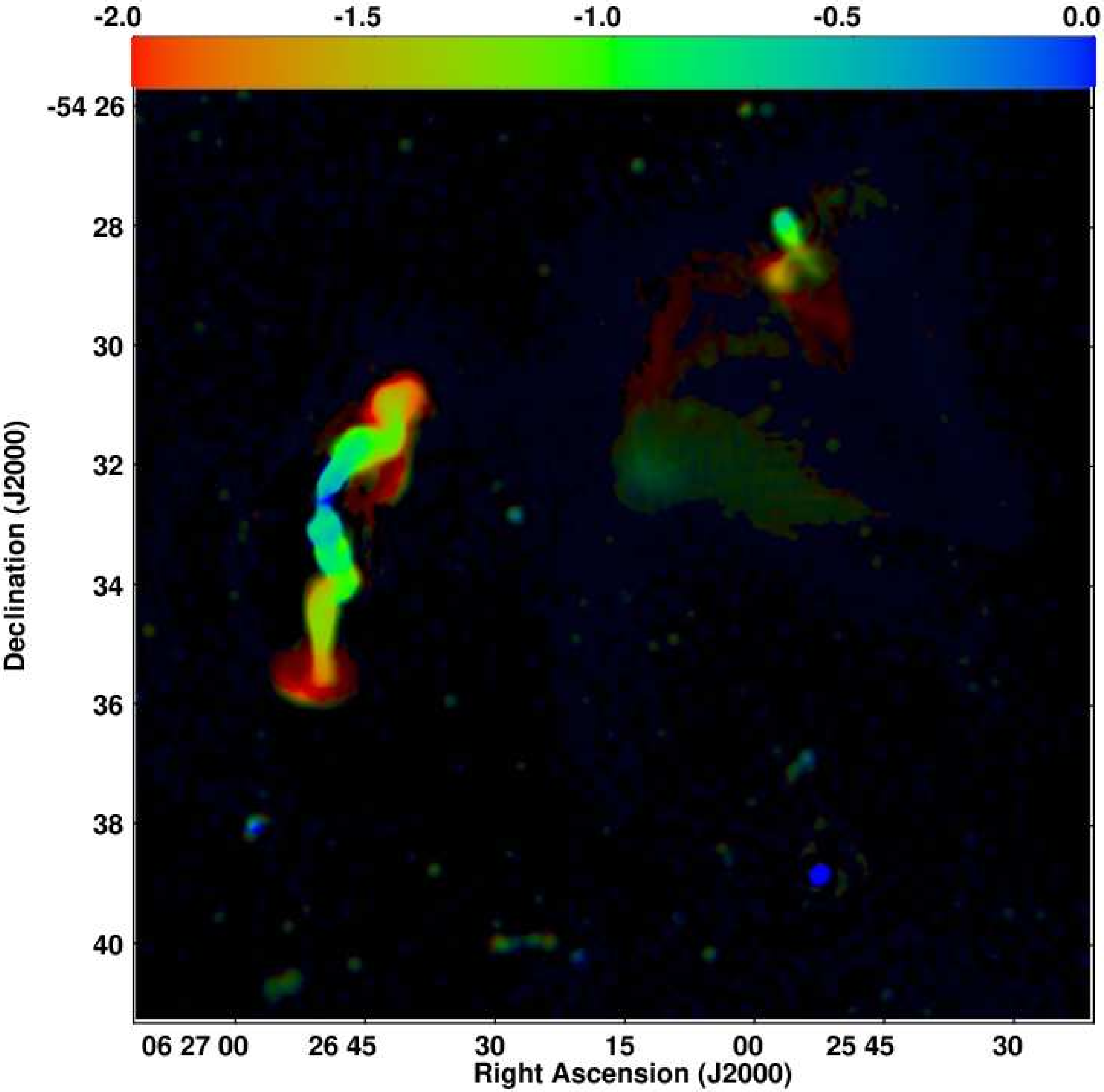


Fig. 7. Brightness and spectral index of center of Abell 3395 as Hue/Intensity. The spectral index is given by the scale bar at the top. The intensity used a $\sqrt{}$ stretch truncated at -50 $\mu$Jy and 10 mJy.

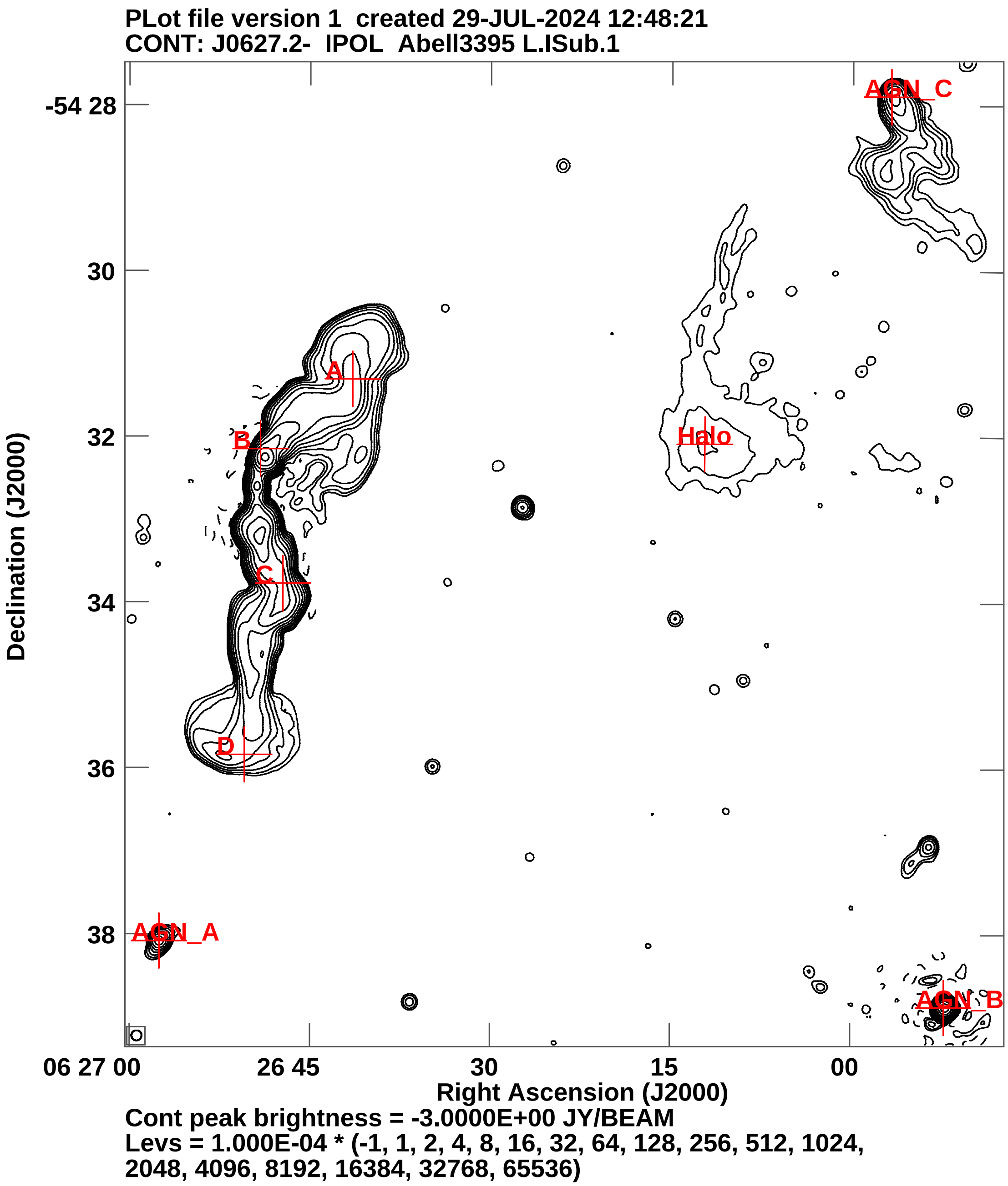


Fig. 8. Contour plot of a region of Abell 3395 in Stokes I marking the locations of various Faraday spectra.

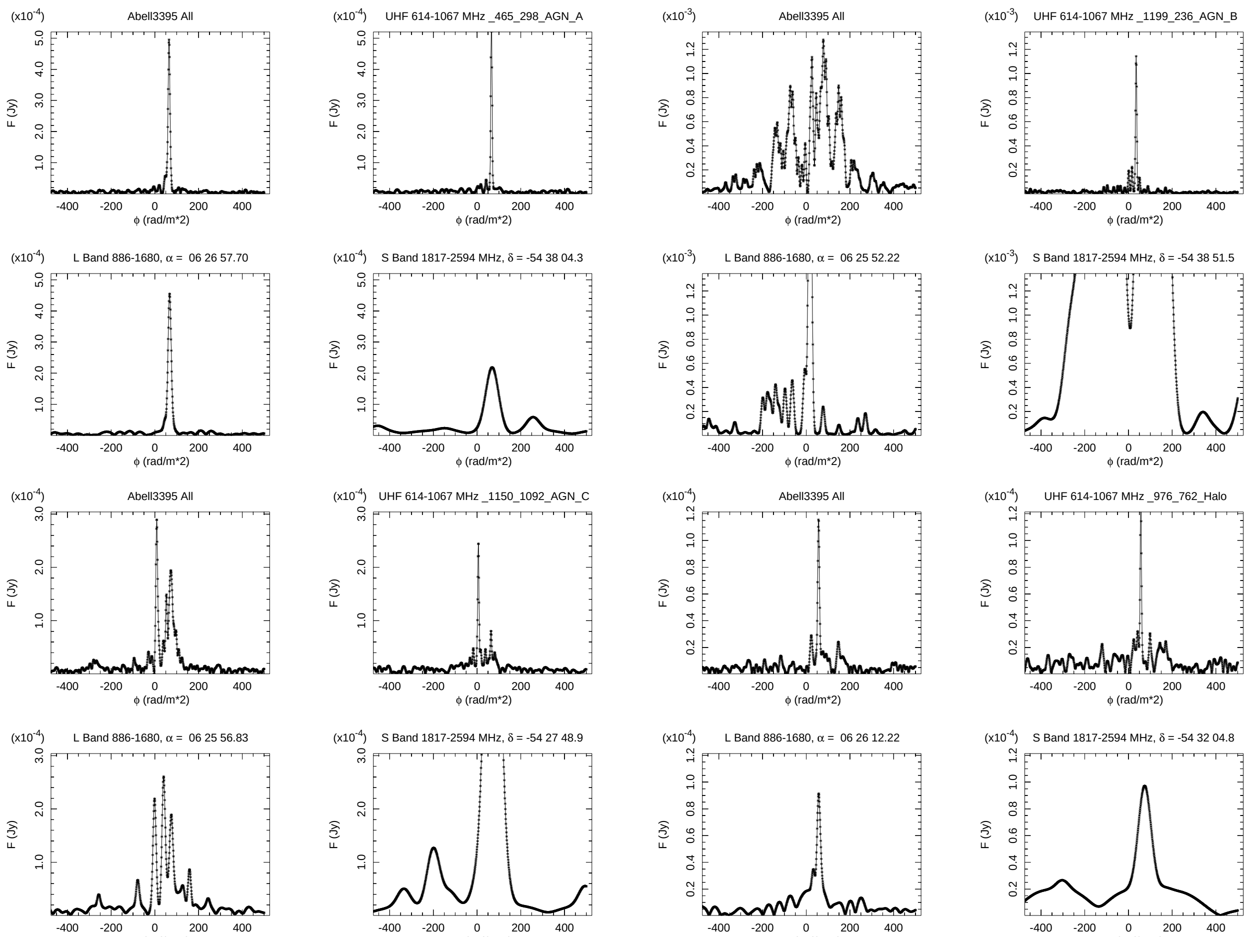


Fig. 9. Faraday Spectra of features indicated in Figure 8. Spectra are shown for the combined data and for each of the bands individually; each panel has 4 plots. **Upper left:** AGN A; **Upper right:** AGN B; **Lower left:** AGN C; **Lower right:** Halo-like feature. All plots in a panel use the same scale.

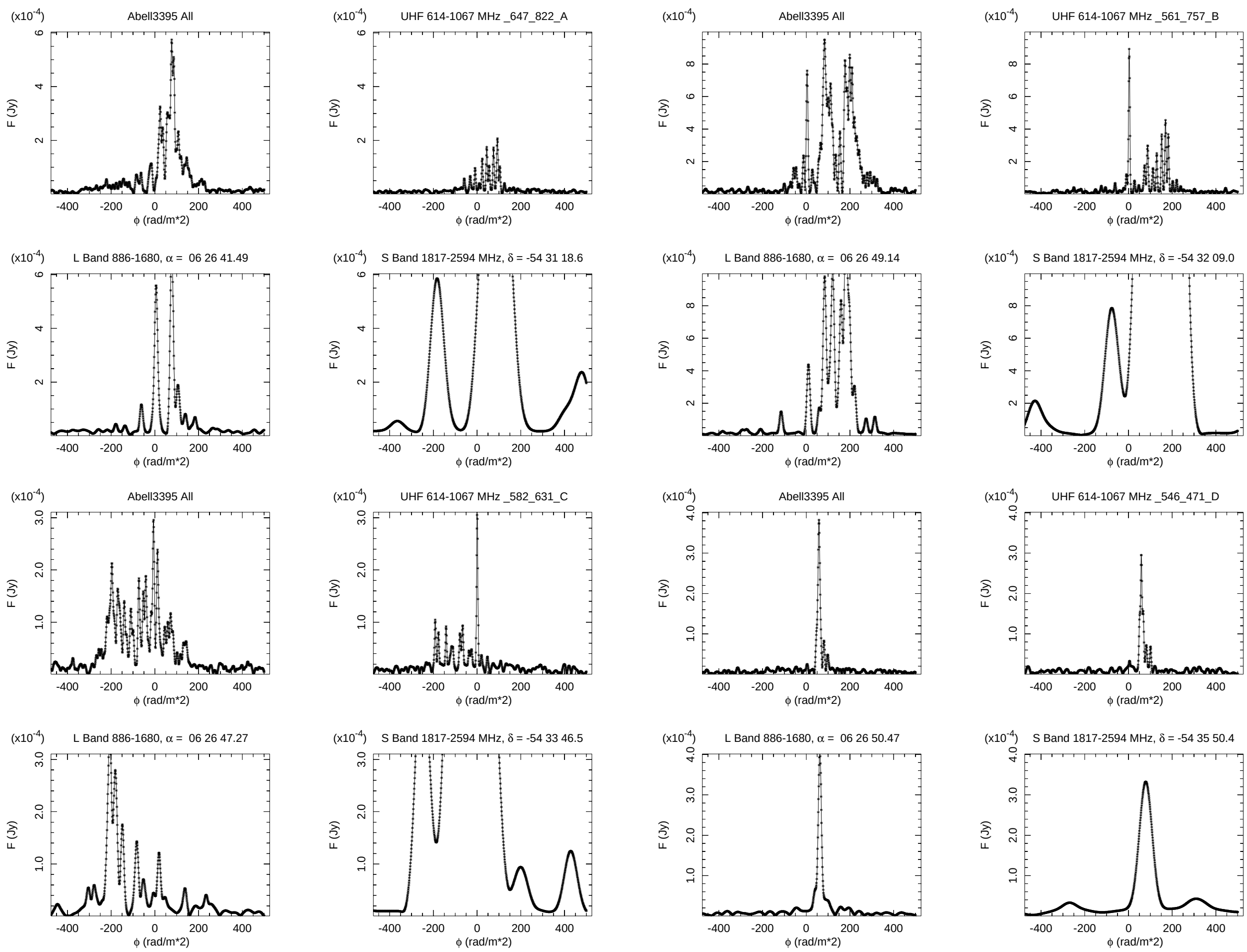


Fig. 10. Further Faraday Spectra at locations in the jet indicated in Figure 8. Spectra are shown for the combined data and for each of the bands individually. **Upper left:** Jet feature A; **Upper right:** Jet feature B; **Lower left:** Jet feature C; **Lower right:** Jet feature D. All plots in a panel use the same scale.

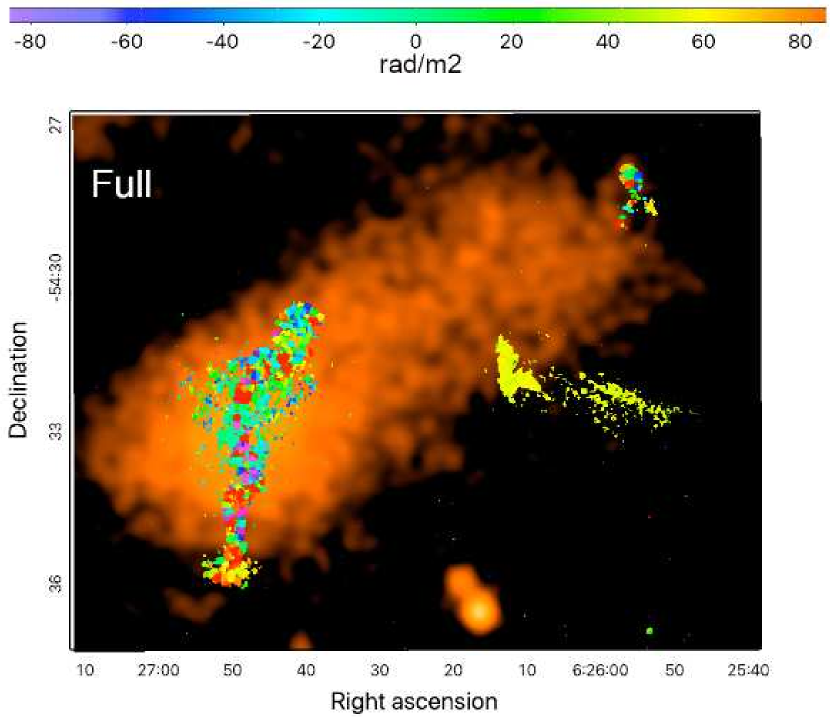


Fig. 11. Abell 3395 with X ray emission as heat map covering a region similar to that in Figure 8. Colors and scale bar at the top give peak rotation measures. From [2].

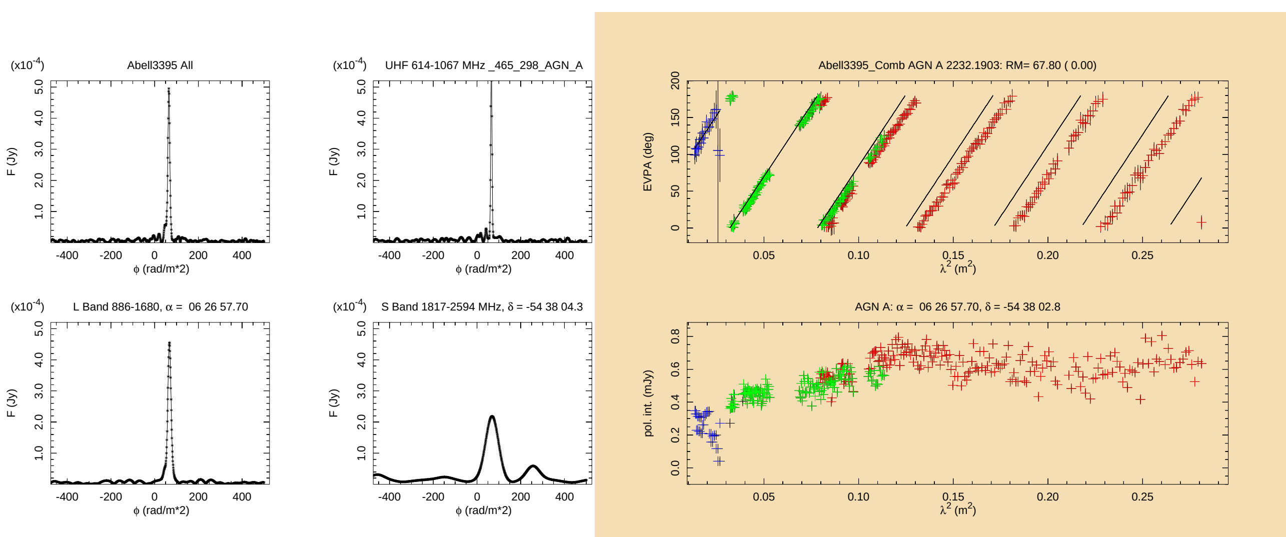


Fig. 12. Faraday and $\lambda^2$ spectra of the source labeled AGN A in Figure 8.
**Left:** Plots as given in Figure 9. All band plots use the same scaling.
**Right:** Spectrum in $\lambda^2$ space. Blue points are S Band, green are L band and red UHF. The solid line represents the Rotation measure fitted to the S Band data.

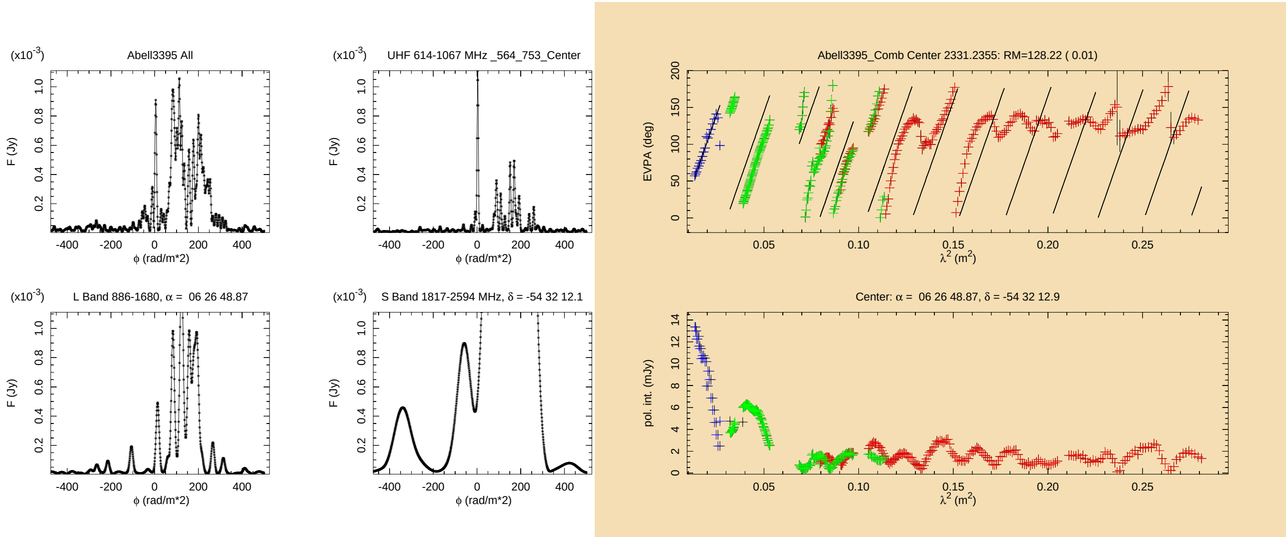


Fig. 13. Like Figure 12 but for position 06 26 48.86 -54 32 12.7.

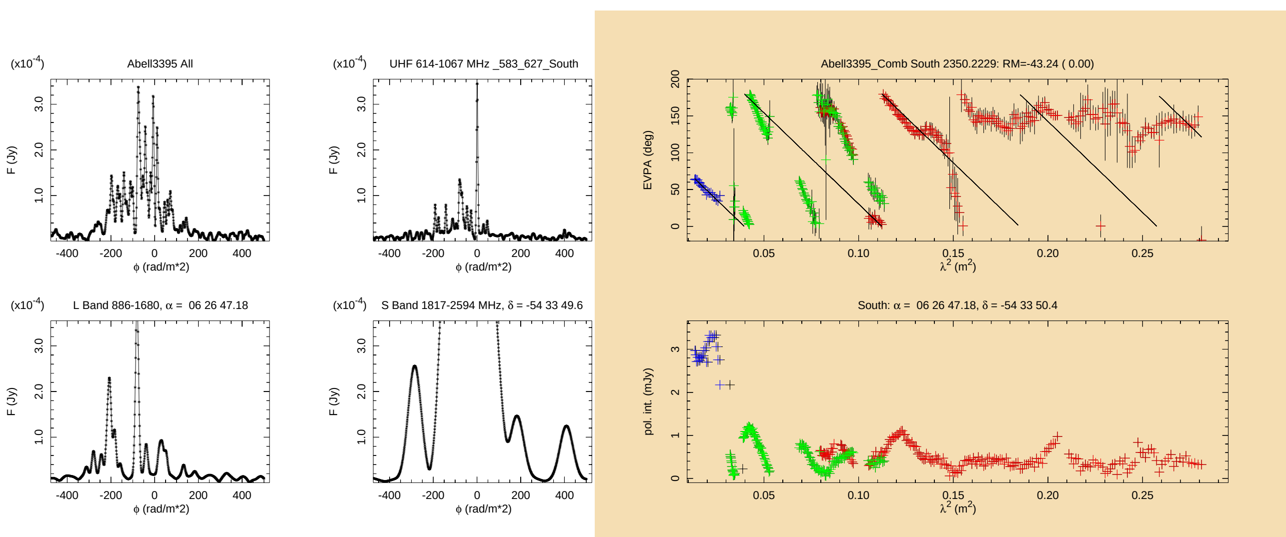


Fig. 14. Like Figure 12 but for position 06 26 47.17 -54 33 50.3.

Fig. 15. Script to determine S Band EVPA corrections

```
# Generate a BP table to correct errors in EVPA derived from a scan on 3C286
# Must be applied to a dataset in circular feed basis (RR,LL,LR,RL)
# AvgBL output with PD and RMDly calibration applied, Circular feed basis
# Averaged over time and baseline (1 vis)
uv=UV.newPAUV('In','J1331+3030_S','Avgnoc',3,1,True,err)
# This file should have a BP table with suitable REAL 2 and IMAG 2 columns

exec(open('HugoPerley_3C286.py').read())
import math
# Want to convert to Stokes IQUV
uv.List.set("Stokes","IQUV")
uv.List.set("doCalSelect",True)
uv.Open(UV.READCAL, err)
vis=uv.ReadVis(err)  # Read data
uv.Close(err)

incs = uv.Desc.Dict['inaxes'][uv.Desc.Dict['jlocs']]
freq0 = uv.Desc.Dict['crval'][2]; dfreq = uv.Desc.Dict['cdelt'][2]
nch = uv.Desc.Dict['inaxes'][2]*uv.Desc.Dict['inaxes'][3]
clight = 2.997924562e8   # Speed of light m/s
rlcorr = []
for i in range(0,nch):
    indx = i*incs;
    nu = freq0 + i*dfreq  # frequency
    lamb = (clight/nu); lamb2 = lamb**2   # Wavelength and squared
    if vis.vis[indx+1][1]>0.0:
        (P,EVPA) = HugoPerley_3C286 (nu)
        q=vis.vis[indx+1][0].real; u=vis.vis[indx+2][0].real;
        evpa = 0.5*math.degrees(math.atan2(u,q))
        #i, nu*1.0e-9, evpa, EVPA, EVPA-evpa
        rlcorr.append(2*math.radians(EVPA-evpa))
    else:
        rlcorr.append(0.0)

bp=uv.NewTable(Table.READWRITE,"AIPS BP",1,err)
bp.Open(Table.READWRITE,err)
nrow = bp.Desc.Dict['nrow']
for j in range(0,nrow):
    row=bp.ReadRow(j+1,err)
    for i in range(0,nch):
        row['REAL 2'][i] = math.cos(rlcorr[i]); row['IMAG 2'][i] = math.sin(rlcorr[i]);

    bp.WriteRow(j+1,row,err)

bp.Close(err)
```